ACS APPLIED MATERIALS & INTERFACES

Research Article

www.acsami.org

Synthesis of Graphene Films by Rapid Heating and Quenching at Ambient Pressures and Their Electrochemical Characterization

L. David,[†] R. Bhandavat,[†] G. Kulkarni,[‡] S. Pahwa,[†] Z. Zhong,[‡] and G. Singh*,[†]

[†]Mechanical and Nuclear Engineering Department, Kansas State University, Manhattan, Kansas 66506, United States

[‡]Department of Electrical Engineering and Computer Science, University of Michigan, Ann Arbor, Michigan 48109, United States

Supporting Information

ABSTRACT: We study the process of graphene growth on Cu and Ni substrates subjected to rapid heating (approximately 8 °C/s) and cooling cycles (approximately 10 °C/s) in a modified atmospheric pressure chemical vapor deposition furnace. Electron microscopy followed by Raman spectroscopy demonstrated successful synthesis of large-area few-layer graphene (FLG) films on both Cu and Ni substrates. The overall synthesis time was less than 30 min. Further, the as-synthesized films were directly utilized as anode material and their electrochemical behavior was studied in a lithium half-cell configuration. FLG on Cu (Cu-G) showed reduced lithium-intercalation capacity when compared with SLG, BLG and Bare-Cu suggesting its substrate protective nature (barrier to Li-ions). Although graphene films on Ni (Ni-G) showed better Li-cycling ability similar to that of other carbons suggesting that the presence of graphene edge planes (typical of Ni-G) is important in effective uptake and release of Li-ions in these materials.

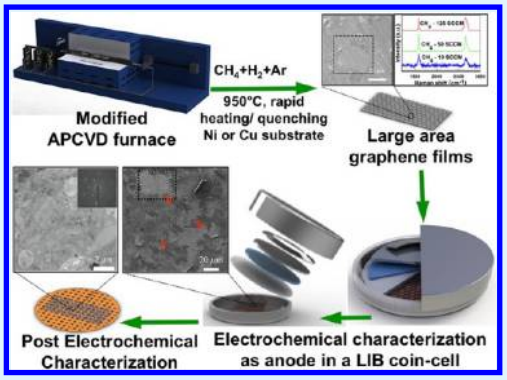

KEYWORDS: *CVD, graphene, rapid heating and cooling and lithium-ion battery*

1. INTRODUCTION

Atomically thin two-dimensional honeycomb lattice structure of graphene and its unique electronic, optical, and mechanical properties are now well-known.[1−6] Several different methods are now available for synthesis of graphene including the mechanical exfoliation,[7] thermal annealing of single-crystal SiC,[8−10] reduction of graphene oxide and low-pressure chemical vapor deposition (LPCVD) on transition metal surfaces with large area.[11,12] LPCVD of carbon on transition metals is the most efficient method for producing large area single or few layer graphene (FLG) films. In fact, researchers at Samsung and Sungkyunkwan University utilized LPCVD to demonstrate synthesis and transfer of very large area (~30-in.) graphene films in a roll-to-roll production process.[13] An even more attractive option is the atmospheric pressure CVD (APCVD) of graphene, which can make this process more accessible and economical. Hence, detailed investigation involving the effect of thermal annealing, substrate type and heating/cooling rates are justified in order to produce high-quality, large-area films consistently and repeatedly.

In addition, there is also a growing interest in exploiting the anticorrosion (protective coatings)[14,15] and Li-adsorption (Li-ion batteries)[16,17] properties of single and FLG films. Recent studies have predicted high Li storage capacity for graphene because of its enormous surface area (~2000 m^2/g),[17] whereas another study has shown negligible Li cycleability for few layer graphene.[16] This could be due to the fact that Li intercalation in graphitic materials can vary depending upon on defect density and stacking between individual layers. Nonetheless, the phenomenon of lithium intercalation in graphene is not fully understood yet.

Hence, the aim of this work was 2-fold: (i) explore the synthesis of large area graphene following rapid heating and quenching at ambient pressures, and (ii) study and correlate the electrochemical lithium cycling ability of the films with their structure. To this end, we were able to synthesize large area graphene films on both copper and nickel substrates. The total synthesis time was reduced from 140 min (for conventional CVD) to less than 30 min. Later, the "as-synthesized" graphene films were utilized as anode material in a lithium-ion battery half-cell and their electrochemical performance was studied and compared with the well-characterized, high-quality, single-layer (SLG), and bilayer (BLG) films prepared by LPCVD process.[18]

2. EXPERIMENTAL SECTION

Materials. Polycrystalline Cu (Alfa Aesar CAS# 7440−50−8, 99.8%) or Ni (Alfa Aesar CAS# 7440−02−0, 99%) foil (25 μm thickness) was cut into 10 × 10 mm^2 pieces and loaded into the furnace. Argon (Ar, purity: 99.999%), hydrogen (H_2, purity: 99.999%) and methane (CH_4, 99.99%) gases were purchased from Matheson Trigas.

CVD/I Method: Slow Heating/Fast Cooling of the Substrate. This process involved heating the substrate to the growth temperature (i.e., 950 °C), at a rate of approximately 15 °C/min in presence of both Ar (at 2000 SCCM) and H_2 (at 300 SCCM). Later, during the

Received: August 24, 2012
Accepted: December 26, 2012
Published: December 26, 2012

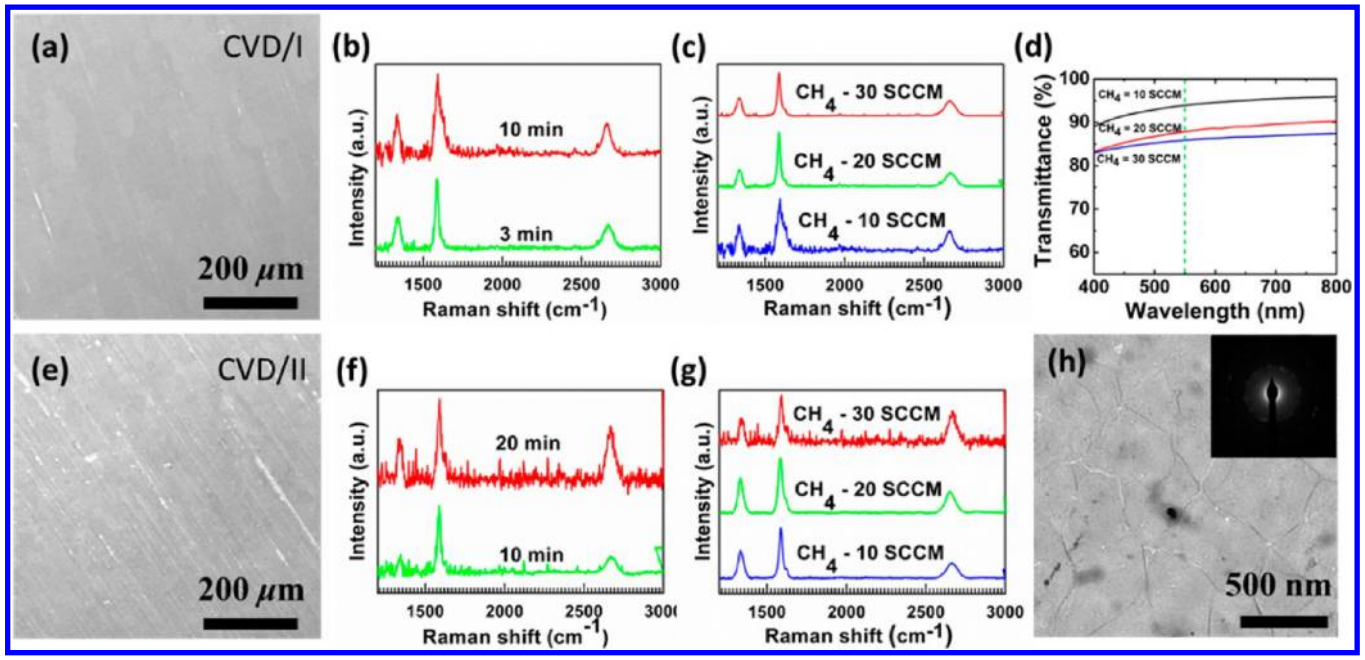

Figure 1. (a–d) SEM, Raman, and UV transmittance data for graphene on Cu synthesized using CVD/I method, respectively. (e–h) SEM, Raman, and TEM data for graphene on Cu synthesized using CVD/II method, respectively. The inset in h is a SAED pattern. See Table S1 in the Supporting Information for more details.

growth period the carbon deposition was initiated with the help of introduction of CH_4 gas at specific flow rates for a specific time. Cooling was carried out at a rate of approximately 10 °C/s (1/60th that of standard procedure). Average total time of synthesis was approximately 70 min. To accommodate this fast cooling rate, the CVD furnace design had to be altered, which is shown in Figure S1 (Supporting Information and animation file). Loading tray in the furnace was replaced with a smaller removable tube inside which the substrate is placed. The gases were redirected through the system such that they first flow into the smaller tube and exhausts out of the system through the other end of the larger concentric tube. This tube-in-tube configuration allowed the substrate to be removed out of the heating zone while still maintaining the inert conditions. The samples were labeled as Cu-950-3-10-C, Cu-950-10-10-C, Cu-950-20-10-C, Cu-950-10-20-C, Cu-950-10-30-C, Ni-950-10-120-C, Ni-950-20-120-C, Ni-950-30-120-C, Ni-950-10-10-C, and Ni-950-10-50-C. The alphabets Cu and Ni indicate Cu and Ni, respectively and the alphabet C at the end of the label indicates that the sample has been cooled fast. The first number stands for the temperature in degree Celsius, the next number indicate the growth time in min and the last number represents the flow rate of methane gas in SCCM during the growth period.

CVD/II Method: Rapid Heating and Quenching of the Substrate. As can been seen in Figure S1 (Supporting Information), the modified furnace design allowed insertion of the growth substrate (placed in the inner tube) directly into the furnace hot zone for quick heating (approximately 8 °C/s). Other growth parameters were similar to those mentioned in CVD/I. The average total time of synthesis using this method was approximately 20 min. These samples were labeled as Cu-950-10-30-HC, Cu-950-20-10-HC, Cu-950-20-20-HC, Cu-950-20-30-HC, Ni-950-10-120-HC, Ni-950-20-120-HC, Ni-950-30-120-HC, Ni-950-10-10-HC, Ni-950-10-50-HC, and Ni-950-10-80-HC. The alphabet HC at the end of the label indicates rapid heating and cooling rate. Details of all other parameters are tabulated in Table S1 in the Supporting Information. Plots representing heating and cooling cycles for CVD/I and CVD/II are shown in Figure S2 in the Supporting Information.

Li-Ion Battery Coin Cell Assembly. Electrochemical behavior of various graphene specimen and bare substrates (Cu or Ni) was studied in a lithium half-cell configuration using a 2032 coin type cell. Batteries were made by punching 14.3 mm diameter out of the as-synthesized foil for use as the working electrode i.e., negative electrode (anode). The electrode was placed on the bottom casing and a drop of electrolyte solution of 1 M $LiPF_6$ (Alfa Aesar) dissolved in (1:1 v/v) dimethyl carbonate (DMC): ethylene carbonate (EC) was then used to wet the top anode surface. A glass separator (19 mm diameter, soaked in the electrolyte) separated the anode from pure lithium metal foil (14.3 mm diameter, 750 μm thick), which acted as the counter electrode. Washer, spring and a top casing were placed on top to complete the assembly before crimping. The complete assembly of the cell was carried out in an Ar-filled glovebox (<1 ppm O_2 and moisture).

Electrochemical performance of the cells was studied using an Arbin test unit sweeping between 10 mV to 2.5 V by applying a constant current density of 5 $\mu A/cm^2$ during both charge and discharge half cycles in atmospheric conditions.

Material Characterization. Scanning electron microscopy (SEM) was carried out by use of a Carl Zeiss EVO MA10 system with incident voltage varying from 5 KV to 30 KV. Raman spectra were measured using a LabRAM ARMIS Raman spectrometer using 633 nm laser excitation (laser power of 17 mW) as the light source. The Raman spectra for all our samples were measured directly on the growth substrate (Ni and Cu), with-in few days after synthesis under same conditions. Transmission electron microscope (TEM) images were digitally acquired by use of a Phillips CM100 operated at 100 KV. TEM and UV samples were prepared by etching away the substrate with suitable solvent (1 M solution of $FeCl_3$ in DI water for Cu and concentrated HNO_3 for Ni) after spin-coating the sample with 1 M solution of PMMA (Polymethyl methacrylate) in toluene and baking it for 10 min in an oven maintained at 120 °C. The graphene sheets attached to PMMA were then transferred to the required substrate. Acetone was then used to dissolve the PMMA. Postcycled TEM was performed in a similar manner; cycled anodes were recovered by dissembling the cells in an Ar-filled glovebox followed by rinsing in DMC solution.

3. RESULTS AND DISCUSSION

Graphene Synthesis Using CVD/I on Cu (Slow Heating/Quenching). Electron microscopy and Raman spectroscopy (λ = 633 nm, 200× objective) were used to analyze the quality and morphology of the synthesized

dx.doi.org/10.1021/am301782h | ACS Appl. Mater. Interfaces 2013, 5, 546–552

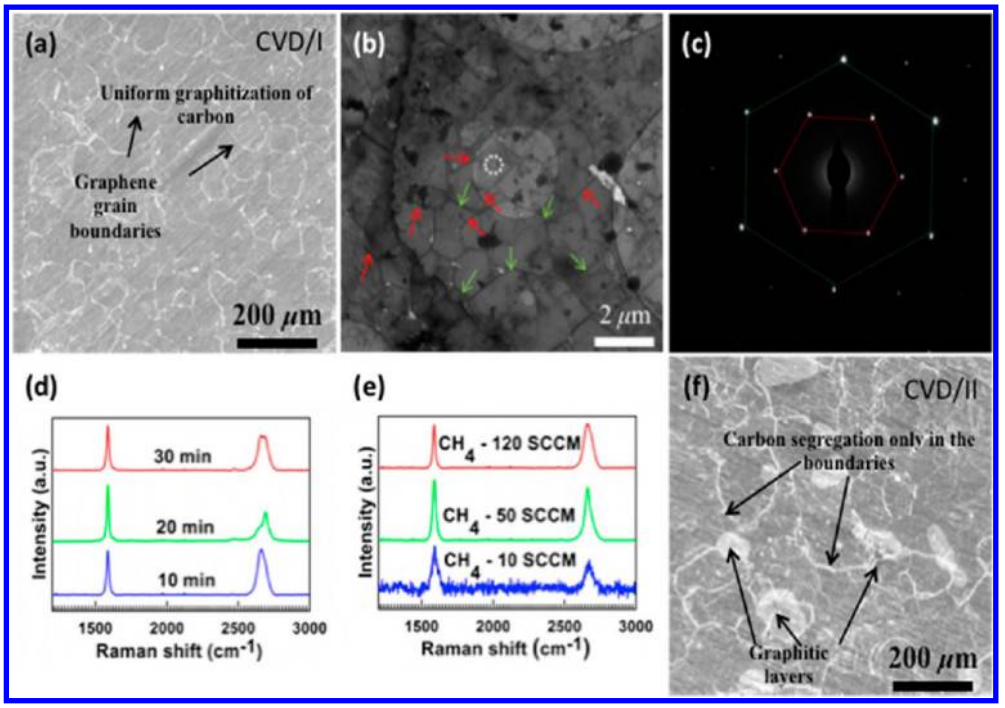

Figure 2. SEM image showing (a) few-layer graphene synthesized on Ni by CVD/I (Ni-950-10-120-C specimen). (b) TEM image (corresponding to a); wrinkles and grain boundaries are indicated by the red and green arrows, respectively. (c) SAED pattern obtained from the spot marked as a circle in the TEM image. (d, e) Raman spectra for CVD/I method, showing the effect of varying growth time (@120 SCCM CH_4) and CH_4 flow rate (growth time of 10 min), respectively. (f) SEM image showing graphitic film produced by CVD/II (Ni-950-10-120-HC specimen) method. The Raman data for CVD/II on Ni is included in Figure S4 (Supporting Information).

graphene films. The SEM image in Figure 1a corresponds to a representative specimen, Cu-950-10-10-C, that showed islands of FLG. These islands looked similar to a previous study on graphene APCVD.[19] The films were more than 100 μm in size and at some areas; they could also be seen as crossing the Cu grain boundaries, indicating formation of a continuous film. Corresponding Raman spectrum is shown in Figure 1b; intense peaks at ~1580 cm^{-1} (G-peak) and ~2700 cm^{-1} (2D-peak) are indicative of two-dimensional sp^2 hybridized carbon structure.[20−29] Presence of D-peak at ~1350 cm^{-1} indicates defective nature of the films, which are again typical of an APCVD process.[23,30−32] The relative intensity of the 2D-peak at ~2700 cm^{-1} with respect to G-peak at ~1580 cm^{-1} (I_{2D}/I_G = 0.39) shows that the graphene films are few layers thick (see Table S1 in the Supporting Information).[30] The optimum growth temperature was observed to be 950 °C.[33,34] No appreciable change was observed in the Raman I_{2D}/I_G ratios when the growth time was varied (Figure 1b). Meanwhile, a decrease in Raman I_{2D}/I_G ratio (Figure 1c) was observed with increasing CH_4 flow rates (from 10 to 30 SCCM), which suggests that the CH_4 flow rate has a predominant effect in determining the number of graphene layers.[19] This observation was corroborated by the UV-transmittance data shown in Figure 1d, the transmittance of graphene films prepared with 10 SCCM of CH_4 was 92%, which decreased to 84% for the specimen prepared at 30 SCCM of CH_4. Thus, approximately 10 min of growth time and 10 SCCM of CH_4 flow rate were observed to be optimum parameters for CVD/I on Cu.

Graphene Synthesis Using CVD/II on Cu (Rapid Heating/Quenching). These experiments showed formation of a relatively defect-free graphene films with large size grains as can be seen in the SEM image (Figure 1e) which corresponds to Cu-950-20-30-HC specimen. Corresponding Raman spectrum in Figure 1f further confirms formation of graphene film, which, based on the I_{2D}/I_G ratio is approximately 3 to 4 layers in thickness.[30] Increasing growth times (Figure 1f) and CH_4 flow rates (Figure 1g) showed increase in Raman I_{2D}/I_G ratio from 0.24 to 0.66 and 0.29 to 0.66, respectively. The TEM image in Figure 1h, also suggests good coverage of the film. In addition, all of the CVD/I and CVD/II specimens showed a single intense 2D (Raman) Lorentzian peak (see Figure S3 in the Supporting Information), which suggests turbostratic stacking with random orientation in different domains.[35] This also corroborates with the polycrystalline SAED (selected area electron diffraction) pattern shown Figure 1h.

Graphene Synthesis CVD/I and II on Ni Substrate. We also utilized the modified furnace to study graphene growth process on Ni substrate. SEM image in Figure 2a corresponds to representative specimen, Ni-950-10-120-C, which showed uniform graphene coverage on Ni. This could also be observed in the corresponding TEM image in Figure 2b. The SAED pattern in Figure 2c could be indexed to single crystal of AB Bernal-stacked graphite with only six spots of reflection being observed in the inner hexagon of 0.223 nm spacing. Edge defects and wrinkles could also be seen. Corresponding Raman spectrum in Figure 2d had an I_{2D}/I_G ratio of 1.03, which suggests that the film was bilayer or a few layers thick and relatively less defective because of the absence of the D-peak.

Further Raman analysis showed (Figure 2d) a decrease in I_{2D}/I_G ratio from 1.03 to 0.78 with increasing growth period from 10 to 30 min (@ 120 SCCM CH_4), respectively. This is attributed to the increased absorption of carbon into the substrate that leads to more number of layers being formed.[36] Changing the flow rate of CH_4 from 10 to 120 SCCM (growth time of 10 min) did not show any measurable change in the Raman spectrum (Figure 2e).

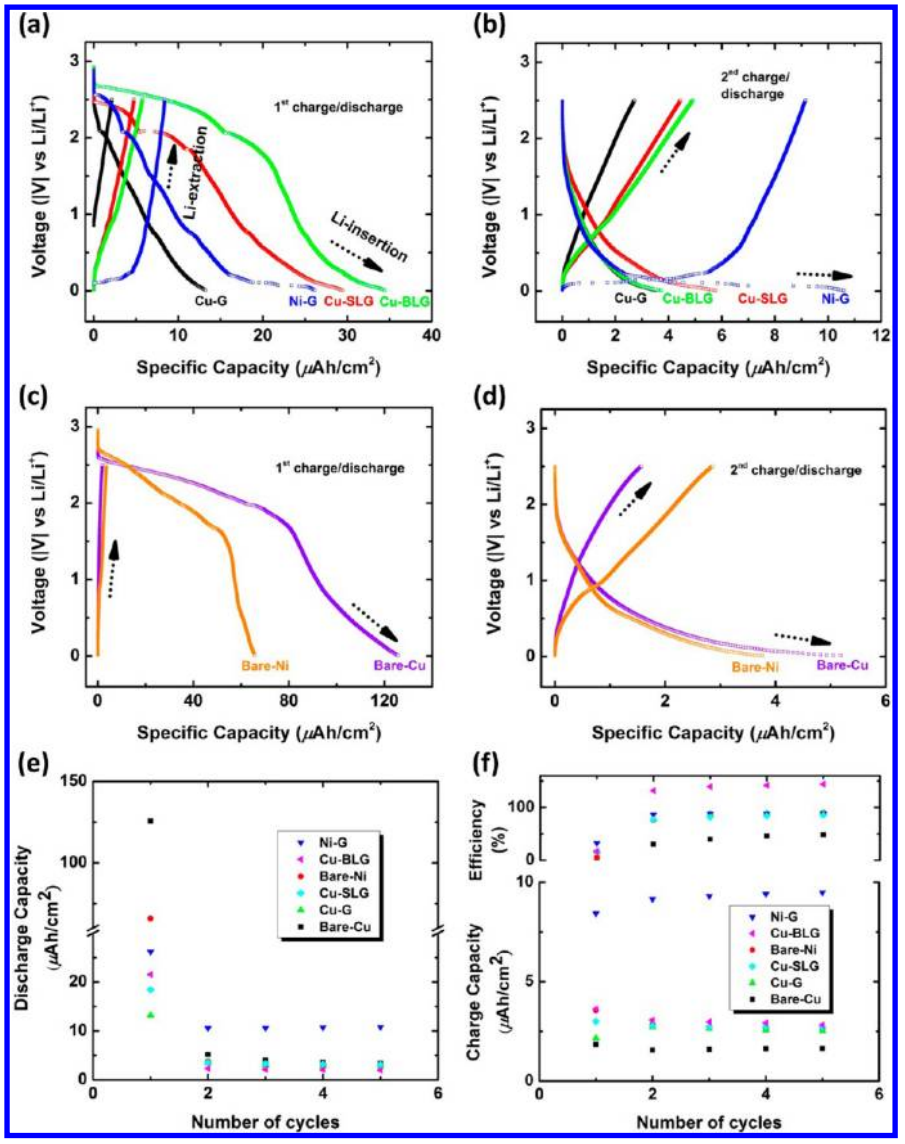

Figure 3. (a, c) First and (b, d) second galvanostatic charge/discharge profiles of various specimens operating at a current rate of 5 μA/cm^2. (e) Discharge and (f) charge capacity (along with the Coulombic efficiency) versus cycle number for various anodes.

CVD/II method, i.e., rapid heating/cooling of the Ni substrate resulted in formation of graphitic carbon as can be seen in Figure 2f. Corresponding Raman data is included in the Supporting Information (Figure S4). One possible explanation could be the reduced annealing time (approximately 2 min), which caused graphene grains to grow as islands thus segregating more carbon in the same area forming graphite. This is illustrated with the help of a schematic in Figure S5 (Supporting Information). The mechanism of graphene growth on Ni is largely a segregation process (particularly at higher growth temperatures)[34,37] and hence the effect of annealing is more pronounced on Ni than on Cu substrate.[38] Also, it seems that the amount of carbon segregating to the surface is determined by the rate of cooling and not by the flow rate of CH_4 during the growth process.[39]

Electrochemical Characterization of Graphene Films. Electrochemical characterization was carried out to understand the lithium intercalation behavior of graphene grown (a) on different substrates and (b) with different number of layers. On the basis of the microscopy and spectroscopy analysis discussed in the previous section, two specimens were selected for electrochemical analysis namely, Cu-950-20-30-HC and Ni-950-10-120-C. From this point, we refer to Cu-950-20-30-HC and Ni-950-10-120-C samples as Cu-G and Ni-G, respectively. Bare-Cu and Ni foils were also fabricated as anode and cycled to differentiate between the intercalation behavior of substrate from the film. In addition, Li-cycling behavior of specimen prepared following well-established LPCVD techniques,[18] i.e., high-quality single-layer (Cu-SLG) and bilayer (Cu-BLG) graphene, was also studied and compared.

The charge/discharge curves for both the first and second electrochemical cycles of all the six anode specimens are shown in Figure 3. The first cycle discharge capacity for Cu-SLG (29.47 μA h/cm^2) and Cu-BLG (34.45 μAh/cm^2) was higher than Cu-G (13.21 μA h/cm^2) but much lower than bare-Cu (125.6 μA h/cm^2), which suggests that the presence of graphene layer acts as a barrier suppressing Li's reaction with the substrate. This means that Cu-G, which is a few layers thick, was more effective in blocking Li-ions reaching the Cu substrate. This observation is in agreement with a recent study that showed Li-intercalation in graphene (grown on Cu) does not start to dominate until it is at least 6−15 layers thick.[16]

dx.doi.org/10.1021/am301782h | ACS Appl. Mater. Interfaces 2013, 5, 546−552

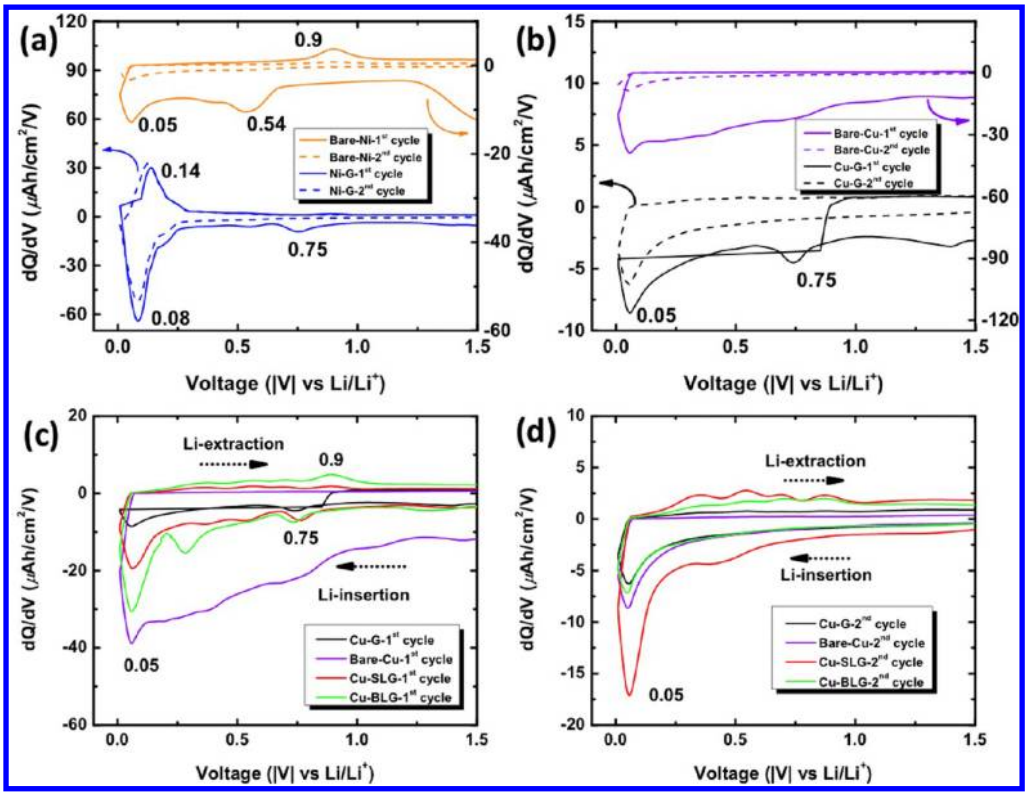

Figure 4. Comparison of first and second cycle differential capacity curve for (a) bare-Ni and Ni-G, and (b) bare Cu and Cu-G anodes. (c) First and (d) second differential capacity curve for all other anodes used in this study.

Also, the first cycle loss for Bare-Cu (Figure 3c, d), was observed to be 98.54%, suggesting limited Li cycleability of metallic Cu.

A similar trend was observed for Ni anodes, the first discharge capacity of Ni-G (26.17 μA h/cm^2) was lower than bare-Ni (65.84 μA h/cm^2) and the first cycle loss for bare-Ni was observed to be very high at 94.59%.

Most importantly, from Figure 3e, f, it can be seen that the cycling behavior of Ni-G anode after the first cycle was quite unique; it showed the highest electrochemical capacity (i.e., charge capacity = 9.5 μA h/cm^2, discharge capacity = 10.7 μA h/cm^2). While all other specimen including bare-Ni cycled close to approximately 2.5 μA h/cm^2. This means that the intercalation of Li-ions in Ni-G is quite distinct than Cu-graphene specimens. Hence, we plotted differentiated capacity curves to understand the underlying differences.

Figure 4a shows the differential capacity curve for Ni-G and Bare-Ni. The Ni-G specimen showed a distinct cathodic (intercalation) peak at 0.08 V and anodic peak at 0.14 V for both first and second cycles, these peaks are typical of lithium intercalation and extraction in carbon materials.[16] In the bare-Ni plot, a cathodic peak at 0.54 V and anodic peak at 0.9 V were observed. These could possibly be due to electrolyte degradation on the electrode surface and were virtually absent in the second cycle indicating that these reactions were irreversible.[16] Similarly, in Figure 4b, which represents differential capacity curve for bare-Cu, only one major peak at ~0.05 V in the first cycle and no other prominent peak in the second cycle were observed (second cycle curve was virtually absent).

To better compare the performance of various graphene−Cu specimens, their first and second cycle differentiated capacity curves are plotted separately in c and d in Figure 4, respectively. As seen in Figure 4c, the intensity of the peak at ~0.05 V was seen for bare-Cu specimen, which then reduced for Cu-G, Cu-SLG and Cu-BLG specimen, while an additional peak centered at ~0.75 V seemed to emerge. This again suggests that increasing number of graphene layers, suppressed Li's reaction with the substrate (i.e., graphene acted as a diffusion barrier). This is more clearly seen in Figure 4d that shows the differentiated capacity curves for the second cycle. Cu-SLG, Cu-BLG, and Cu-G showed peaks at ~0.05 V, indicating that some intercalation of Li-ions was allowed through the graphene film (possibly through the basal planes). These specimens also did not show any distinct anodic peaks and the intensity of the cathodic peak (for Cu-G) at ~0.05 V was approximately six times less than that of Ni-G specimen.

These results indicate low cycleability and the protective nature (against Li-salts) of the graphene films grown on Cu substrate. Related layer-dependent capacities are mentioned in Table 1.

Later, the cells were disassembled and the anodes recovered for further characterization. The SEM image in Figure 5 shows the pre- (above, a−d)- and post-cycled (below, e−h) anode surfaces. In all cases, the SEI (solid electrolyte interphase) formation and increased spacing at the graphene grain boundaries due to repeated cycling of Li ions could be observed. The contamination in the images is that of the residue glass separator material. Also, these anodes may have been exposed to air during the transfer process resulting in oxidation of Li ions, which appeared as bright spots in the images (due to their nonconducting nature). In Figure 5e−h, these bright spots are mostly observed on the grain boundaries, which are labeled by the red arrows. This was further confirmed by the TEM images in Figure 5i−l, in which the dark spots suggest evidence of intercalation near the grain boundaries. It

dx.doi.org/10.1021/am301782h | ACS Appl. Mater. Interfaces 2013, 5, 546−552

Table 1. Summary of the Electrochemical Data

sample	capacity (μAh/cm^2) 1st cycle discharge	1st cycle charge	2nd cycle discharge	2nd cycle charge	1st cycle efficiency (%)
Cu-G	13.21	2.16	3.48	2.72	16.38
Ni-G	26.17	8.43	10.59	9.15	32.21
Cu-SLG	29.47	4.8	5.77	4.46	16.29
Cu-BLG	34.45	5.8	3.73	4.91	16.83
bare-Cu	125.6	1.83	5.17	1.6	1.46
bare-Ni	65.84	3.56	3.77	2.86	5.41

can be noted that the intensity of these dark spots increased as the number of layers increases from Figure 5(i-l) and in Ni-G specimen, the dark spots are primarily concentrated to the grain boundaries. In addition, more grain boundaries were observed for Ni-G (average grain size of ~10 μm) than Cu-G (average grain size ~30 μm) specimen, which could also be the reason for the increased intercalation capacity of Ni-G.

The results of electrochemical analysis allow us to postulate possible mechanisms for lithium intercalation in graphene. The defect sites and the grain boundaries on the basal plane are most likely the paths for Li ion intercalation in Cu-SLG, Cu-BLG, and Cu-G. In addition, the turbostratic nature of the Cu-G specimen could be the reason for limited Li-cycling observed in these specimens. The better Li-cycleability observed for the Ni-G specimen is collectively attributed to its smaller domain size (i.e., more grain boundaries for Li diffusion) and the presence of multilayer graphene (with Bernel stacking) near its grain boundaries, providing multiple paths for efficient storage and release of Li-ions.

4. CONCLUSION

We have demonstrated synthesis of large area FLG films on poly-Cu and Ni in a modified APCVD furnace under rapid heating and cooling conditions. We were able to reduce the overall synthesis time to less than 30 min while maintaining optimum quality as demonstrated by Raman spectroscopy. Further, electrochemical behavior of the substrates with graphene films was studied in a Li-ion half-cell configuration as anode material. A considerable decrease in first cycle Li intercalation was observed when compared to their bare counterparts proving graphene's substrate-protective nature. Only graphene grown on Ni was able to cycle Li-ions in a continuous manner, with charge−discharge profile matching that of other carbon materials. Electron microscopy of the cycled anodes showed increased accumulation (possibly Li-species) near the grain boundaries, which imply that Li intercalation is dependent on density of defect sites, plane type and stacking order. Finally, conclusions obtained in this work would allow rapid manufacture of graphene films in an economical manner for a wide range of applications particularly corrosion resistant and longer-lasting battery electrodes.

■ ASSOCIATED CONTENT

Supporting Information

Description related to graphene synthesis and summary of the results. This material is available free of charge via the Internet at http://pubs.acs.org.

■ AUTHOR INFORMATION

Corresponding Author

*E-mail: gurpreet@ksu.EDU. Tel.: +1-785-532-7085. Fax: +1-785-532-7057.

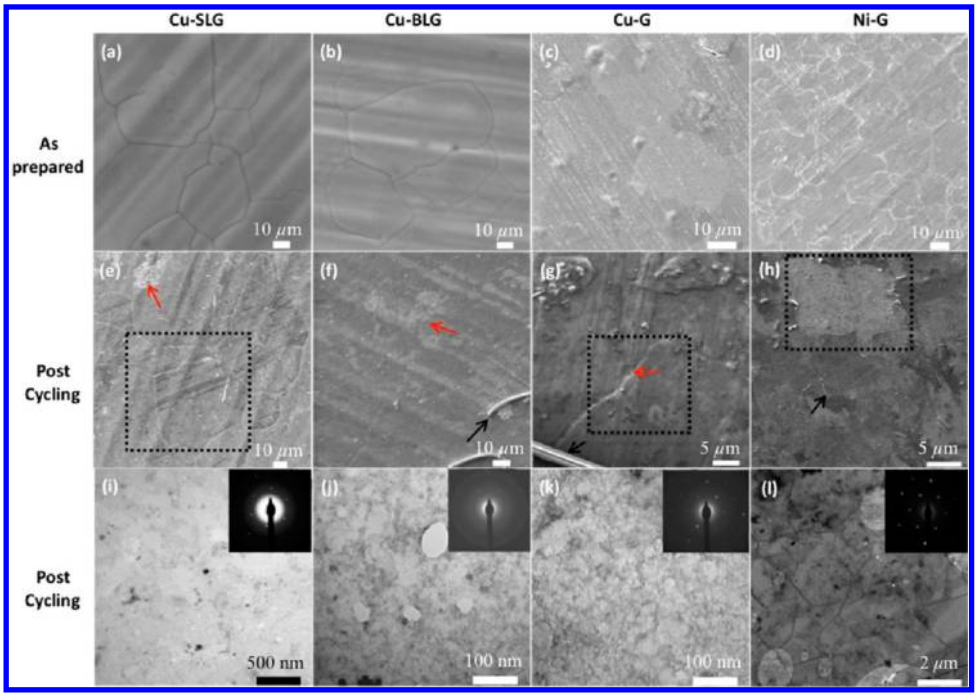

Figure 5. SEM images of as-prepared (top) and postcycled surfaces (below) of (a, e) Cu-SLG, (b, f) Cu-BLG, (c, g) Cu-G, and (d, h) Ni-G anodes. Dotted box indicate graphene grains/boundaries, black arrow represents separator membrane impurity, and red arrow indicates bright spots (possibly oxidized Li-species at defect sites), which are also observed as dark spots in the TEM images: (i) Cu-SLG, (j) Cu-BLG, (k) Cu-G, and (l) Ni-G anodes.

dx.doi.org/10.1021/am301782h | ACS Appl. Mater. Interfaces 2013, 5, 546−552

Notes

The authors declare no competing financial interest.

■ ACKNOWLEDGMENTS

G.S. thanks Dr. Elisabeth Mansfield and Dr. Stephanie Hooker of the National Institute of Standards and Technology-Boulder Laboratories for help with the chemical vapor deposition furnace. Thanks are also due to Professors R. Raj and J. Scott Bunch (University of Colorado at Boulder) for useful discussions related to graphene synthesis. Z.Z. acknowledges support from National Science Foundation Scalable Nanomanufacturing Program (DMR-1120187).

■ REFERENCES

(1) Geim, A. K.; Novoselov, K. S. *Nat. Mater.* **2007**, *6*, 183−191.
(2) Sun, Z.; James, D. K.; Tour, J. M. *J. Phys. Chem. Lett.* **2011**, *2*, 2425−2432.
(3) Rangel, N. L.; Seminario, J. M. *J. Phys. Chem. A* **2008**, *112*, 13699−13705.
(4) Lu, Y. H.; Chen, W.; Feng, Y. P.; He, P. M. *J. Phys. Chem. B* **2008**, *113*, 2−5.
(5) Lee, C.; Wei, X.; Kysar, J. W.; Hone, J. *Science* **2008**, *321*, 385−388.
(6) Chen, S.; Wu, Q.; Mishra, C.; Kang, J.; Zhang, H.; Cho, K.; Cai, W.; Balandin, A. A.; Ruoff, R. S. *Nat. Mater.* **2012**, *11*, 203−207.
(7) Novoselov, K. S.; Geim, A. K.; Morozov, S. V.; Jiang, D.; Zhang, Y.; Dubonos, S. V.; Grigorieva, I. V.; Firsov, A. A. *Science* **2004**, *306*, 666−669.
(8) Morgan, A. E.; Somorjai, G. A. *Surf. Sci.* **1968**, *12*, 405−425.
(9) Van Bommel, A. J.; Crombeen, J. E.; Van Tooren, A. *Surf. Sci.* **1975**, *48*, 463−472.
(10) Hass, J.; Feng, R.; Li, T.; Li, X.; Zong, Z.; Heer, W. A. d.; First, P. N.; Conrad, E. H.; Jeffrey, C. A.; Berger, C. *Appl. Phys. Lett.* **2006**, *89*, 143106.
(11) Li, X.; Cai, W.; An, J.; Kim, S.; Nah, J.; Yang, D.; Piner, R.; Velamakanni, A.; Jung, I.; Tutuc, E.; Banerjee, S. K.; Colombo, L.; Ruoff, R. S. *Science* **2009**, *324*, 1312−1314.
(12) Sutter, P. W.; Flege, J. I.; Sutter, E. A. *Nat. Mater.* **2008**, *7* (5), 406−411.
(13) Bae, S.; Kim, H.; Lee, Y.; Xu, X.; Park, J. S.; Zheng, Y.; Balakrishnan, J.; Lei, T.; Ri Kim, H.; Song, Y. I.; Kim, Y. J.; Kim, K. S.; Ozyilmaz, B.; Ahn, J. H.; Hong, B. H.; Iijima, S. *Nat. Nanotechnol.* **2010**, *5*, 574−578.
(14) Chen, S.; Brown, L.; Levendorf, M.; Cai, W.; Ju, S.-Y.; Edgeworth, J.; Li, X.; Magnuson, C. W.; Velamakanni, A.; Piner, R. D.; Kang, J.; Park, J.; Ruoff, R. S. *ACS Nano* **2011**, *5*, 1321−1327.
(15) Prasai, D.; Tuberquia, J. C.; Harl, R. R.; Jennings, G. K.; Bolotin, K. I. *ACS Nano* **2012**, *6*, 1102−1108.
(16) Yao, F.; Güneş, F.; Ta, H. Q.; Lee, S. M.; Chae, S. J.; Sheem, K. Y.; Cojocaru, C. S.; Xie, S. S.; Lee, Y. H. *J. Am. Chem. Soc.* **2012**, *134*, 8646−8654.
(17) Kaskhedikar, N. A.; Maier, J. *Adv. Mater.* **2009**, *21*, 2664−2680.
(18) Lee, S.; Lee, K.; Zhong, Z. *Nano Lett.* **2010**, *10*, 4702−4707.
(19) Bhaviripudi, S.; Jia, X.; Dresselhaus, M. S.; Kong, J. *Nano Lett.* **2010**, *10*, 4128−4133.
(20) Ferrari, A. C. *Solid State Commun.* **2007**, *143*, 47−57.
(21) Ferrari, A. C.; Meyer, J. C.; Scardaci, V.; Casiraghi, C.; Lazzeri, M.; Mauri, F.; Piscanec, S.; Jiang, D.; Novoselov, K. S.; Roth, S.; Geim, A. K. *Phys. Rev. Lett.* **2006**, *97*, 187401.
(22) Hao, Q.; Wang, B.; Bossard, J. A.; Kiraly, B.; Zeng, Y.; Chiang, I. K.; Jensen, L.; Werner, D. H.; Huang, T. J. *J. Phys. Chem. C* **2012**, *116*, 7249−7254.
(23) Ferrari, A. C.; Robertson, J. *Phys. Rev. B* **2000**, *61*, 14095.
(24) Cuesta, A.; Dhamelincourt, P.; Laureyns, J.; Martínez-Alonso, A.; Tascón, J. M. D. *Carbon* **1994**, *32*, 1523−1532.
(25) Bacsa, W. S.; de Heer, W. A.; Ugarte, D.; Châtelain, A. *Chem. Phys. Lett.* **1993**, *211*, 346−352.
(26) Gruber, T.; Zerda, T. W.; Gerspacher, M. *Carbon* **1994**, *32*, 1377−1382.
(27) Jawhari, T.; Roid, A.; Casado, J. *Carbon* **1995**, *11*, 1561−1565.
(28) Ivleva, N. P.; Messerer, A.; Yang, X.; Niessner, R.; Pöschl, U. *Environ. Sci. Technol.* **2007**, *41*, 3702−3707.
(29) Stankovich, S.; Dikin, D. A.; Piner, R. D.; Kohlhaas, K. A.; Kleinhammes, A.; Jia, Y.; Wu, Y.; Nguyen, S. T.; Ruoff, R. S. *Carbon* **2007**, *45*, 1558−1565.
(30) Dresselhaus, M. S.; Jorio, A.; Hofmann, M.; Dresselhaus, G.; Saito, R. *Nano Lett.* **2010**, *10*, 751−758.
(31) Malard, L. M.; Pimenta, M. A.; Dresselhaus, G.; Dresselhaus.. *Phys. Rep.* **2009**, *473*, 51−87.
(32) Lu, A. Y.; Wei, S. Y.; Wu, C.-Y.; Hernandez, Y.; Chen, T.-Y.; Liu, T.-H.; Pao, C.-W.; Chen, F.-R.; Li, L.-J.; Juang, Z.-Y. *RSC Adv.* **2012**, *2* (7), 3008−3013.
(33) Sinclair, R.; Itoh, T.; Chin, R. *Microsc. Microanal.* **2002**, *8*, 288−304.
(34) Zheng, M.; Takei, K.; Hsia, B.; Fang, H.; Zhang, X.; Ferralis, N.; Ko, H.; Chueh, Y. L.; Zhang, Y.; Maboudian, R.; Javey, A. *Appl. Phys. Lett.* **2010**, *96*, 063110−063110−3.
(35) Ni, Z.; Wang, Y.; Yu, T.; You, Y.; Shen, Z. *Phys. Rev. B* **2008**, *77* (23), 235403.
(36) Huang, L.; Chang, Q. H.; Guo, G. L.; Liu, Y.; Xie, Y. Q.; Wang, T.; Ling, B.; Yang, H. F. *Carbon* **2012**, *50*, 551−556.
(37) Weatherup, R. S.; Bayer, B. C.; Blume, R.; Baehtz, C.; Kidambi, P. R.; Fouquet, M.; Wirth, C. T.; Schlögl, R.; Hofmann, S. *ChemPhysChem* **2012**, *13* (10), 2544−2549.
(38) Yu, Q.; Lian, J.; Siriponglert, S.; Li, H.; Chen, Y. P.; Pei, S. S. *Appl. Phys. Lett.* **2008**, *93*, 113103.
(39) Reina, A.; Thiele, S.; Jia, X.; Bhaviripudi, S.; Dresselhaus, M.; Schaefer, J.; Kong, J. *Nano Res.* **2009**, *2*, 509−516.